(Technical Note) The effective calibration of a Multi-Modal C-arm Fluoroscope

Xin Chen, Hemal Naik, Lejing Wang, Nassir Navab and Pascal Fallavollita

Chair for Computer Aided Medical Procedures, Fakultät für Informatik,Technische Universität München, München, Germany
{chenxin, naik, wangle, fallavol}@in.tum.de;
{navab@cs.tum.edu}

ABSTRACT

The multi-modal C-arm fluoroscope augments an X-ray image with optics providing a real-time in-situ overlay of the anatomy to the surgeon. The correctness of the overlay is crucial for intra-operative guidance, thus a precise calibration of the multi-modal C-arm device is required. The current calibration procedure is composed of three steps with the first being the most complex as it involves the determination of the X-ray source position. This step is performed using a biplane phantom and is currently guided by the acquisition of many X-ray images—a task that is both time-consuming and radiation intensive. In this technical note, a real-time solution is proposed which takes advantage of optic guidance to drive the calibration process thereby minimizing both X-ray and time involved. Eight users with varying calibration expertise were asked to participate in the evaluation of our optic-guided calibration technique. Results demonstrated that our new calibration process dramatically reduces the number of X-ray images required by 79.6%, decreases the total time required by 42%, and utilizes ideally only one X-ray image for the entire calibration. In conclusion, we showed that the optical-guided calibration ensures a timely, quasi radiation-free calibration of the multi-modal C-arm fluoroscope and offers friendly guidance to non-experts.

Keywords: *Multi-modal technology, X-ray, Optics, Calibration, Computer Vision*

1. INTRODUCTION

In the last decade, the first medical augmented reality (AR) technologies enhancing the direct view of the surgical target with virtual data were introduced. Most in-situ visualization systems augment the view of a surgeon or an optical camera with pre-operative data based on image registration techniques. Preoperative data however cannot represent the real-time anatomical information. For this, intra-operative imaging has been employed for medical augmented reality, since the images can be updated impromptu during surgery. What follows is a brief literature review describing some of these systems.

Stetten *et al*. (2005) present a real-time tomographic reflection system which augments a single ultrasound image of the anatomy with its surface based on a half silvered mirror and a flat panel miniature monitor. Fichtinger *et al*. (2005) propose an intra-operative medical AR system for visualizing one CT slice onto the patient in-situ via a specific arrangement of half transparent mirror and monitor rigidly attached to a CT scanner. A similar technique was proposed for the in-situ visualization of a single MRI slice by Fischer *et al.* (2007). Wendler *et al*. (2007) fuse real-time ultrasound images with synchronized real-time functional nuclear information from a gamma probe based on optical tracking in a common coordinate system. Feuerstein *et al*. (2008) augment laparoscope optic images with intra-operative 3D cone-beam CT by tracking a C-arm fluoroscope and laparoscope using the same external optical tracking system.

The accurate positioning and pose determination of a C-arm fluoroscopy device to other modalities can be achieved with tracking technologies that combine radiographic fiducials as seen in Moult *et al*. (2010) and Fallavollita *et al*. (2010).

1.1 The Multi-Modal C-arm Fluoroscope

The majority of intra-operative technologies requires either tracking techniques, hindered by line of sight issues, and requires a specific and complex arrangement of the imaging devices in order to align the different images or viewing geometries.

Recently, Navab *et al.* (1999, 2010) developed the Camera Augmented Mobile C-arm (CamC), or AR Fluoroscope, which enhances a standard mobile C-arm device by an optical camera and mirror construction. Both X-ray source and optical centers are virtually aligned at the same position so that both can have the same view of the patient (Figure 1, Figure 2).

Figure 1. The CamC consists of a mirror and optical camera add-on affixed to the X-ray housing of a standard mobile C-arm fluoroscope.

From this, an intuitive in-situ intra-operative overlay between X-ray and optic images is achieved. With the X-ray augmented by live video, surgeons can now perform operations more confidently with less radiation exposure, reduced rate of potential surgical mistakes, and increased reproducibility. Wang *et al*. (2010a) published the first results of CamC on

forty patients during 2009-2010 allowing it to become the first medical AR technology used in real surgeries worldwide. Moreover, the co-registered overlay allows for many computer-assisted surgery (CAS) solutions such as: parallax-free X-ray image stitching by Wang *et al.* (2010b), visual servoing based C-arm down-the-beam positioning by Navab *et al*. (2006), C-arm 6 DOF kinematic modeling by Wang *et al.* (2012a), radiation-free guidance of interlocking of intramedullary nails procedures by Diotte *et al.* (2012), and the measurement of mechanical axis deviation by Wang *et al.* (2012b) and Brand *et al.* (2012). Nevertheless, the major drawback of the system lies in its complex calibration process. This limitation becomes apparent if the system becomes mis-calibrated prior to or during surgery at which point a stoppage in procedure occurs.

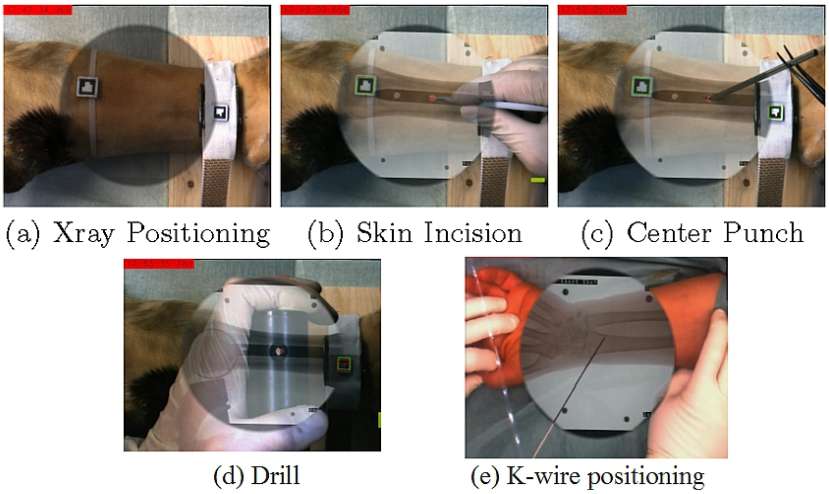

Figure 2. Sample overlay visualizations and surgical applications on animal cadaver leg and human arm.

1.2 Contributions

This technical note provides an elegant and simple solution to absolve the most complex calibration step of the multi-modal C-arm fluoroscope. An inexperienced user may require more than 15 X-ray images to complete this calibration step in which the X-ray source position is determined. We propose a new method that takes advantage of real-

time optical guidance for the quick and accurate calibration of the camera augmented mobile C-arm. We validated our solution by involving eight probands in performing the calibration using the existing method compared to our new technique. We recorded and assessed: (i) the total number of X-ray image acquisitions required and (ii) total amount of time in minutes.

2. The original calibration process

Proposed by Navab *et al.* (2010), a biplane phantom was designed to determine the position of X-ray source prior to the virtual alignment of the optic camera center to it. The sequential steps for calibration are summarized below.

First, the X-ray source center is determined by the intersection of at least two distinct linear rays (five pairs are used here), each of which is defined by two distinct points: the movable metallic rings on the top layer and the fixed X-ray visible markers on the bottom layer (Figure 3-left). The existing calibration method can only provide guidance based on X-ray images until all five metallic rings on the top layer are moved to the position where all five markers on the bottom layer can be seen through five rings (iso-centric) as shown in Figure 3-right. This step needs many X-ray acquisitions, is very time consuming, and is considered a "*trial and error*" process (i.e. move metallic rings and acquire X-ray, confirm overlay, repeat, etc.).

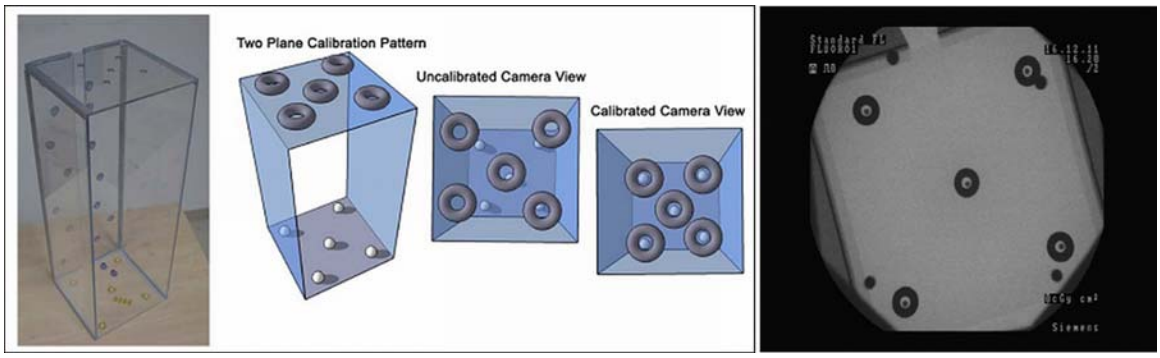

Figure 3. (*Left*) The biplane phantom used in the first step of the calibration process. By a "trial and error" sequence, upper rings are moved and aligned with the fixed markers at the bottom of the phantom via many X-ray image acquisitions. (*Right*) The final X-ray image shows confirmation of iso-centricity thereby determining X-ray position.

Second, the mirrors are moved to align the optic and X-ray centers. The X-ray source and the optical camera center are aligned if and only if the five markers on the bottom layer can also be seen through five rings (iso-centric) in the optic images (Figure 4). This process requires is fast and requires only a few seconds.

Third, after successful alignment of X-ray source and optical camera center, a universal non-plane-dependent homography $\boldsymbol{H} \in R^{3x3}$ can be calculated by: (i) using either the calibration matrices of the X-ray and optical camera, together with the rotation matrix between them, or (ii) using point correspondence between X-ray and optic images as presented in Chen *et al.* (2012).

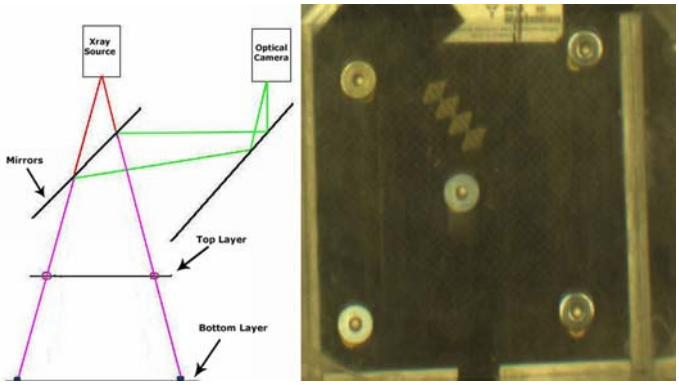

Figure 4. (*Left*) The markers on the bottom layer can be seen through the rings on the top layer if the X-ray source (source of red beams) and the optical camera center (source of green beams) are virtually aligned (pink beams). (*Right*) The alignment of five pairs of markers and rings in the video image.

3. Video-guided calibration

3.1 New calibration workflow

As it is shown in the flowchart of Figure 5, any point $\mathbf{I_x} \in \mathbf{Img_{xray}}$ of plane π can be transferred to $\mathbf{I_v} \in \mathbf{Img_{video}}$ and vice versa once the homography **H** is obtained. From the iso-centric property of the rings and markers in the final X-ray image, we know that the position of the rings in the final X-ray image can be determined if all the markers can be detected using optics. If this is the case, the homography of the upper plane of the calibration phantom can be used to map the position of rings to their position in the optic images. First, the homography ($\mathbf{H_{xv}}$) of the top plane can be calculated through the center positions of the rings in both X-ray ($\mathbf{R_x}$) and video images ($\mathbf{R_v}$) such that any points on top plane of the calibration phantom, in the X-ray image, can be transferred to the video image:

$$I_v = H_{xv} * I_x \qquad (1)$$

Second, the destination of the rings in the X-ray image ($\mathbf{M_x}$) is the centers of markers ($\mathbf{P_{xy}}$) because of the iso-centric property. The points ($\mathbf{P_{xy}}$) in the X-ray image ($\mathbf{M_x}$) are then transferred to the video image ($\mathbf{M_v}$) by the homography ($\mathbf{H_{xv}}$). The points ($\mathbf{M_v}$) are finally plotted on the graphical user interface (GUI) of the existing multi-modal fluoroscopy system. Lastly, the user will manually guide the rings to position ($\mathbf{M_v}$) using the GUI and video augmentation. This in turn signifies that the rings have been correctly positioned in the X-ray image.

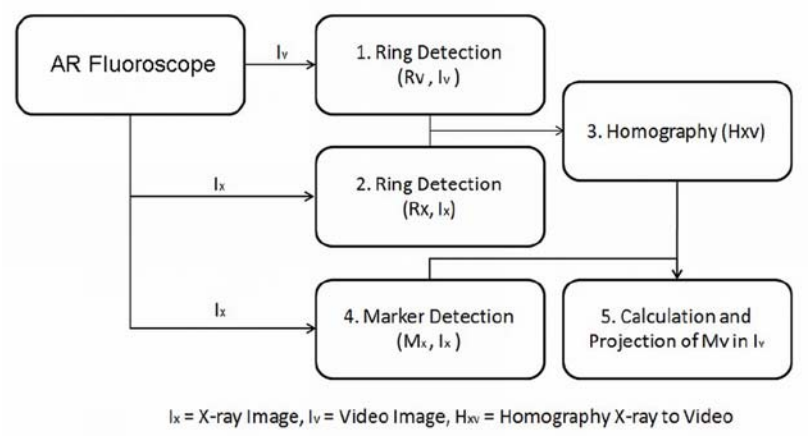

Figure 5. The video-guided calibration workflow steps.

3.2 Video-guided calibration algorithm

The position of rings and markers in either X-ray or video images is detected by using libraries provided by OpenCV. Our algorithm is implemented as an additional feature to the existing GUI framework of the multi-modal fluoroscopy system. Video augmentation of the target position of rings are developed using OpenGL libraries. The circular rings are colored black to enhance the contrast, thus simplifying their detection in the optic images. Since the internal parameters (i.e. focus, brightness, etc.) of the attached video camera to the C-arm do not change, the algorithm parameter values listed below were determined empirically and are considered robust for our system.

Step 1: Detection of Rings in Video Image: Ring centers in the video image have to be detected. To simplify this process a contour detection algorithm is used. The contour detection algorithm uses a binary image obtained by thresholding (threshold = 10) the grayscale video image over a suitable intensity value. First, all detected contours are filtered based on their size (i.e. the sizes of the ring are known *a priori*). Then, those contours are processed with an ellipse fitting method to identify false positives from the

true rings. Lastly, the approximate centers of the circular rings (Rv) are found. Figure 6-left shows a white circle drawn inside the detected rings representing the center points (i.e. details of the selection criteria for a contour identification: area > 150, eccentricity of contour < 1.5 and ellipse fitting accuracy < 3).

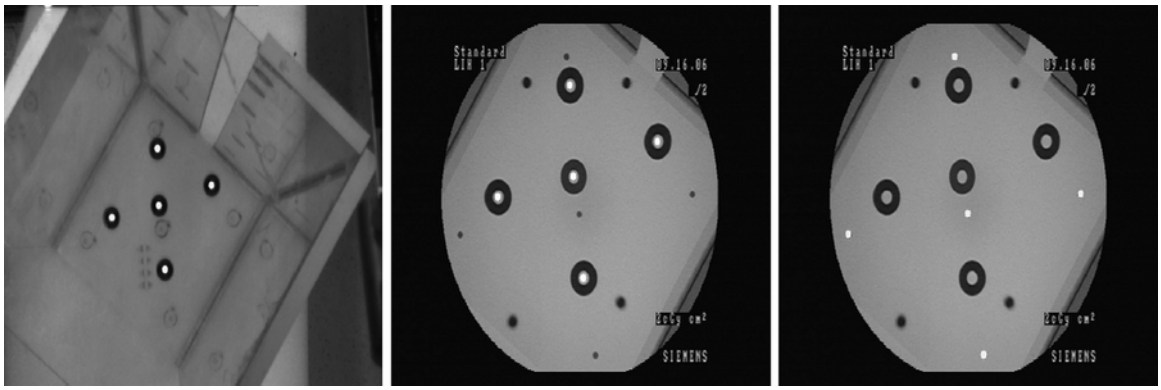

Figure 6. (*Left*): Centers of rings in the optic image displayed as white dots. (*Center*): Centers of rings in the X-ray image displayed as white dots. (*Right*): Centers of fixed biplane markers in the X-ray image shown as white dots.

Step 2: Detection of Rings in the X-ray Image: Using a similar method, but with a different threshold value (threshold = 80), the center of rings in the X-ray image (Rx) is identified. Figure 6-center shows the detected points.

Step 3: Detection of Markers in the X-ray Image: Using the same algorithm as in Step 1, marker positions in X-ray images are identified. Markers are detected by modifying the filtering process during contour detection based on the fact that the marker sizes are considerably smaller than the circular rings. We obtain a new set of points which are displayed in Figure 6-right.

Step 4: Calculation of Homography: In OpenCV, the origin of the image is defined as the top left corner of the image. The X-axis of the coordinates is defined by the top left and

top right corners and the direction points from the top left corner to the top right corner. The Y-axis is defined in the same way by the vector that points from top left corner to bottom left corner together with the origin. The contours detection is performed following the top-down and left-right routine. Thus, when all five rings are detected in both X-ray and video images, the corresponding points are determined by the order of the rings detection. Using these point correspondences, the homography $\mathbf{H_{xv}}$ is calculated.

Step 5: Ring positions for video-based augmentation: Using the homography obtained in Step 4, points $\mathbf{M_x}$ are transferred to $\mathbf{M_v}$. Points $\mathbf{M_v}$ is augmented as '+' sign in the GUI. There is a circle drawn surrounding the '+' to help the user manually position the rings. Note: Rings are placed arbitrarily on the top plane prior to calibration. The algorithm begins working when all five markers are detected in the X-ray image and all five rings are detected in both X-ray and video images.

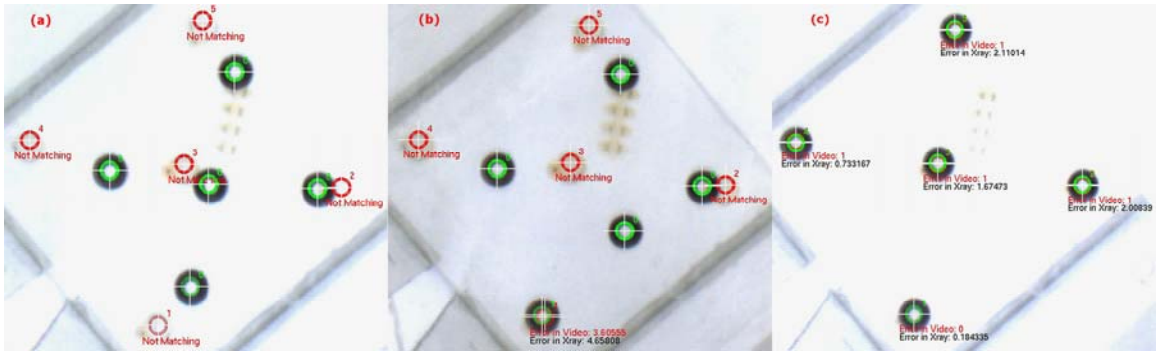

Figure 7. The GUI showing the target positions of the five rings in red alongside the five metallic rings drawn in green. All detections are performed in real-time. Each circle representing the target position and each ring have a number of its own shown (#1-#5) in its north east direction. "*Not Matching*" are shown under each of the red circles representing the target positions. If the ring is moved to the place where the distance between the ring and the target position is smaller than 5 pixels, the number of the green circle is set equal to the number of the red circle. Both video overlay and reprojection error in X-ray (i.e. pixels) are shown in red and black respectively. When the distance of each of the five rings in the video image is no more than 1 pixel, the calibration process is considered completed.

3.3 The graphical user interface (GUI)

The aim of our proposed video-guided calibration is to assist the user in moving the rings on the top layer to the position where the fixed X-ray visible markers become isocentric— in an intuitive and quick manner. The final position ($\mathbf{M_v}$) of the five rings in video images can be calculated as stated above. Points $\mathbf{M_v}$ are defined by the intersection of two orthogonal white lines ('+') as shown in (Figure 7-left). Red circles, whose centers are points $\mathbf{M_v}$, are drawn in video images as the target destination of the rings. The centers of rings are detected in real-time and defined by the same white crosses. The rings detected in real-time are marked by green circles in order to be distinguished from the target points. Each point of $\mathbf{M_v}$ has a number of its own and shown in its north east direction. Each ring also has the same number as the point of $\mathbf{M_v}$ if it is moved into the neighborhood of a point of $\mathbf{M_v}$. Here the neighborhood is defined as the area inside the circle whose center is any point of $\mathbf{M_v}$ and < 5 pixels away. When any one of the rings is moved into the neighborhood of a marker, the distance between the center of the ring and the corresponding point of $\mathbf{M_v}$, which is defined as residual non-iso-centric error, is shown in real-time under the red point in the video image. The re-projection error in the X-ray image calculated by the homography is also shown in real-time (Figure 7-center) in black. For each point of $\mathbf{M_v}$, the calibration is completed when the residual non-iso-centric error of all the five pairs of rings and target positions is at most 1 pixel in the video image (Figure 7-right). This value holds and is equivalent in delivering a reliable multi-modal C-arm fluoroscopic overlay to the surgeon, as discussed in Wang *et al.* 2012.

4. Evaluation & Results

Eight probands were asked to perform the AR fluoroscope calibration using the existing technique based on X-ray guidance alone vs. the proposed video-guided calibration as described in this technical note. In total, 4 participants never performed calibration (i.e. novice group), 2 participants performed calibration only once using the existing technique (i.e. semi-expert group) and 2 participants are experienced users of the existing calibration technique (i.e. expert group). The metrics that were considered during the evaluation are: (i) total number of X-ray image acquisitions to complete calibration, and (ii) total amount of time in minutes. The workflow steps for both calibration methods are described below:

4.1 Existing calibration procedure workflow (WF)

1. *Begin clock and X-ray count.*
2. *WF1: Position randomly the five metallic rings on the top layer of the biplane phantom and take one X-ray shot.*
3. *WF2: Move the rings towards their destination according to the X-ray image on the screen. Acquire an X-ray image for confirmation.*
4. *WF3: If any pair of 5 rings and markers is not iso-centric, repeat WF2 until quasi perfect superposition.*
5. *End clock and X-ray shot count.*

4.2 Video-guided calibration using 1 X-ray

1. *Begin clock and X-ray count.*
2. *WF1: Position randomly the five metallic rings on the top layer of the biplane phantom.*
3. *WF2: Take an X-ray shot. If any of the five markers is overlayed by the rings in the X-ray image, go back to WF1.*
4. *WF3: Start the video guidance calibration program and GUI. Overlay rings accordingly as in Fig. 7.*
5. *WF4: When distance between each ring and its target destination in video is < 1 pixel, calibration is considered complete.*

optional steps which are not mandatory and require additional X-rays

6. *WF5: User has the option of acquiring an additional X-ray shot to confirm superposition.*

7. WF6: If the user thinks they can improve the superposition-- move ring(s) accordingly and take additional X-ray shot(s) until satisfied. The additional #X-ray shots and time in this step are called as additional X-ray acquisitions and time respectively.
8. End clock and X-ray shot count.

The supplemental video assigned with this paper demonstrates the key differences between the existing calibration and the proposed video-guided method. The average time and number of X-ray images required to complete the first step of the AR fluoroscope calibration using the existing method compared to the proposed video-guidance calibration technique is depicted in Figure 8. Our evaluation showed statistical significance. The number of X-ray acquisitions required to complete the calibration decreased by 82% for the novice group, 84% for the semi-expert group and 73% for the expert group. The total time required for the calibration decreased by 56% for the novice group, 53% for the semi-expert group and 17% for the expert group. The number of X-ray shots and time for the optional verification stage of marker/ring superposition, in section 3.2, are also included.

5. Discussion and Conclusions

In this technical note we have proposed an elegant solution to calibrate accurately an augmented reality fluoroscope that is currently used to assist navigation and completion of orthopedic and trauma procedures. We exploit the optic feedback of the multi-modal C-arm fluoroscopy system by detecting rings in real-time which assists the user in aligning accurately both the X-ray and optic camera centers. The GUI offers a visual of the non-isocentric pixel errors between movable circular rings and their target destinations as the user manually moves the rings. During the experiments we asked 8

participants to achieve at most 1 pixel error iso-centricity for each of the 5 rings. In the perfect scenario, a quasi-perfect overlay error via video can be achieved (i.e. ~ 0 pixels).

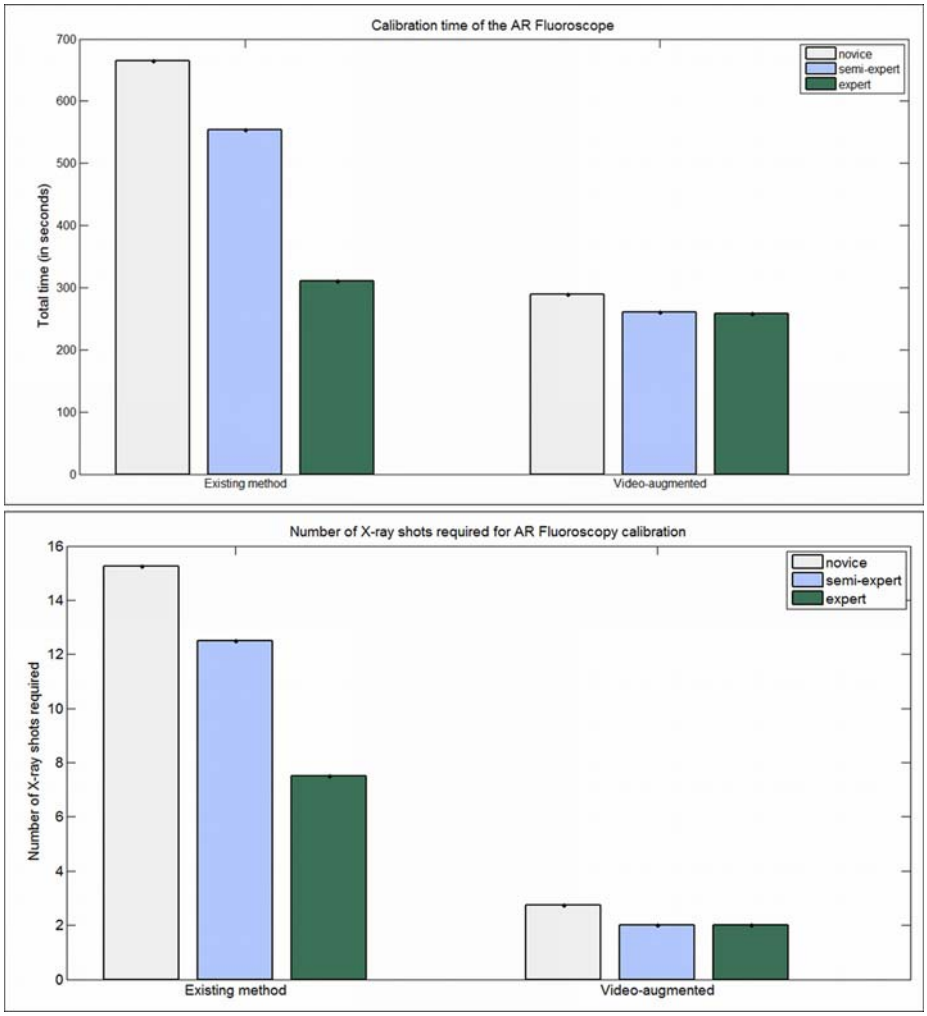

Figure 8. The total time (*top*) and the total number of X-ray shots required (*bottom*) to complete the first of three steps of the calibration of the AR fluoroscope using the existing method vs. the new calibration guidance method.

By training the end user we hypothesize a quicker calibration. The calibration process can now be completed by acquiring only one X-ray shot using our proposed video-guidance calibration technique. Until now, the existing AR fluoroscopy system calibration was time consuming and required many X-ray images. This is a problem if the AR fluoroscope were to become miscalibrated prior to or during surgery (i.e. due to mirrors being unintentionally moved, etc.). From the evaluation, our video augmented calibration

dramatically reduces the number of X-ray images required by 79.6%, and decreases the total time required by 42%. In conclusion, we showed that the existing calibration process of the multi-modal fluoroscope was complex however by exploiting the optic camera we can assist and guide any users by video guidance to achieve desired overlay results in less time with minimal exposure to X-ray.

References

- *Stetten et al. (2005).* Stetten G, Cois A, Chang W, Shelton D, Tamburo R, Castellucci J and von Ramm O 2005 C-mode real-time tomographic reflection for a matrix array ultrasound sonic flashlight *Academic Radiology* **12** 535–543
- *Fichtinger et al. (2005).* Fichtinger G, Deguet A, Masamune K, Balogh E, Fischer GS, Mathieu H, Taylor RH, Zinreich SJ and Fayad LM 2005 Image overlay guidance for needle insertion in CT scanner *IEEE Transactions on Bio-Medical Engineering* **52** 1415–1424
- *Fischer et al. (2007).* Fischer GS, Deguet A, Csoma C, Taylor RH, Fayad L, Carrino JA, Zinreich SJ and Fichtinger G 2007 MRI image overlay: application to arthrography needle insertion *Computer Aided Surgery: Official Journal of the International Society for Computer Aided Surgery* **12** 2–14
- *Wendler et al. (2007).* Wendler T, Feuerstein M, Traub J, Lasser T, Vogel J, Daghighian F, Ziegler SI and Navab N 2007 Real-time fusion of ultrasound and gamma probe for navigated localization of liver metastases *Med Image Comput Comput Assist Interv* **10** 252–260

- *Feuerstein et al. (2008).* Feuerstein M, Mussack T, Heining SM and Navab N 2008 Intraoperative laparoscope augmentation for port placement and resection planning in minimally invasive liver resection *IEEE Transactions on Medical Imaging* **27** 355–369
- *Moult et al. (2011).* Moult E, Burdette EC, Song DY, Abolmaesumi P, Fichtinger G and Fallavollita P 2011 Automatic C-arm pose estimation via 2D/3D hybrid registration of a radiographic fiducial. *Proc. SPIE Int. Soc. Opt. Eng* **7964** 79642S
- *Fallavollita et al. (2010).* Fallavollita P, Burdette EC, Song D, Abolmaesumi P and Fichtinger G 2010 C-arm pose estimation in prostate brachytherapy by registration to ultrasound *Med Image Comput Comput Assist Interv* **13(3)** 311-8
- *Navab et al. (1999).* Navab N, Mitschke M and Schütz O 1999 Camera-Augmented Mobile C-arm (CAMC) Application: 3D Reconstruction Using a Low-Cost Mobile C-arm *Med Image Comput Comput Assist Interv* **1679/1999** 688-697.
- *Navab et al. (2010).*Navab N, Heining S M and Traub J 2010 Camera Augmented Mobile C-Arm (CAMC): Calibration, Accuracy Study, and Clinical Applications *IEEE Transactions on Medical Imaging* **29(7)** 1412-1423
- *Wang et al. (2010a).*Wang L, Landes J, Weidert S, Blum T, von der Heide A, Euler E and Navab N 2010 First Animal Cadaver Study for Interlocking of Intramedullary Nails under Camera Augmented Mobile C-arm *Information Processing in Computer-Assisted Interventions* **6135/2010**, 56-66
- *Wang et al. (2010b).*Wang L, Traub J, Weidert S, Heining S M, Euler E and Navab N 2010 Parallax-free intraoperative X-ray image stitching *Medical Image Analysis* **14(5)** 674-686

- *Navab et al. (2006).*Navab N, Wiesner S, Benhimane S, Euler E and Heining SM 2006 Visual servoing for intraoperative positioning and repositioning of mobile C-arms *Med Image Comput Comput Assist Interv* **19(1)** 551-560
- *Wang et al. (2012a).*Wang L, Fallavollita P, Zou R, Chen X, Weidert S and Navab N 2012 Closed-Form Inverse Kinematics for Interventional C-Arm X-Ray Imaging With Six Degrees of Freedom: Modeling and Application *IEEE Trans Med Imaging* **31(5)** 1086-99
- *Chen et al. (2012).*Chen X, Wang L, Fallavollita P and Navab N 2012 Precise X-ray and video overlay for augmented reality fluoroscopy *Int J Comput Assist Radiol Surg* 1-10
- *Diotte et al. (2012).*Diotte B, Fallavollita P, Wang L, Weidert S, Thaller P, Euler E and Navab N 2012 Radiation-free drill guidance in interlocking of intramedullary nails. *Med Image Comput Comput Assist Interv* **7510/2012** 18-25
- *Wang et al. (2012b).*Wang L, Fallavollita P, Brand A, Erat O, Weidert S, Thaller PH, Euler E and Navab N 2012 Intra-op measurement of the mechanical axis deviation: an evaluation study on 19 human cadaver legs *Med Image Comput Comput Assist Interv* **7511/2012** 609-616
- *Brand et al. (2012).*Brand AG, Wang L, Fallavollita P, Sandner P, Navab N, Euler E, Thaller PH and Weidert S 2012 Intraoperative measurement of mechanical axis alignment by automatic image stitching: a human cadaver study *International Society for Computer Assisted Orthopaedic Surgery (CAOS)*